20th Australasian Fluid Mechanics Conference
Perth, Australia
5-8 December 2016

Experiment Design and Characterization for the Study of Afterbody Radiation during Mars Entry

S.Gu[1], R.G. Morgan[1], T.J. McIntyre[2], and A.M. Brandis[3]
[1]School of Mechanical and Mining Engineering, The University of Queensland, Brisbane, Queensland, 4072, Australia
[2]School of Mathematics and Physics, The University of Queensland, Brisbane, Queensland, 4072, Australia
[3] AMA Inc, NASA Ames Research Center, Moffett Field, California, 94035, USA

Abstract

Recent work has shown that a significant contributor to the afterbody aeroheating during Mars entry is radiation [1, 2, 3]. However, relevant ground test data is not available to help assess the uncertainty associated with prediction of the radiation when designing the thermal protection system for the aeroshell afterbody. The present work is aimed at designing an experiment which allows the study of the afterbody radiation experienced during Mars entry. The X2 expansion tube at the University of Queensland is used to generate the relevant experimental freestream flow conditions. Analysis is carried out to accurately characterize the generated experimental freestream conditions. A two dimensional wedge model is used to produce the expanding flow which simulates aspects of the afterbody flow around Mars entry vehicles. Preliminary analysis of the generated expanding flow shows that it produces significant radiation in the mid-infrared region and has a steady duration of about 50-110 μs. This allows emission spectroscopy to be conducted in the future.

Introduction

The sizing of the afterbody thermal protection system (TPS) for Mars entry has previously been made by considering only convective heating [4]. Radiative heating has been ignored as it has been considered to be insignificant. This assumption has now been shown to be invalid as the radiative heating has been found to be of the same order of magnitude as the convective heating [1, 2, 3, 5, 6]. So although the afterbody radiative heating is small compared to the heating on the forebody, it is still significant compared to what the afterbody TPS is designed for, especially when uncertainties are considered. Hence, it is important to account for this radiative heat flux when sizing the afterbody TPS for future mission design. However the validation of radiative heating in expanding flows is currently limited by the lack of experimental data.

Previous Work

Radiating carbon dioxide expanding flows not been studied experimentally in the past. However, work has been done numerically in simulating the afterbody radiation during Mars entry. The first available study of the effects of the afterbody radiation during Mars entry was performed by Gromov and Surzhikov in 2002 [6]. Their results showed that the afterbody radiative heat flux is of a comparable value to the afterbody convective heat flux, for velocities under 6 km/s. In their study, the highest afterbody radiative heat flux corresponded to a velocity of 4 km/s. In 2011, Lino da Silva and Beck performed axisymmetric, two temperature simulations of the EXOMARS capsule [5]. They showed that the afterbody radiation during Mars entry is produced by carbon dioxide molecules emitting in the mid infrared region. This explains the cause of the afterbody radiation magnitude peaking at around 3-4 km/s. These findings were supported in a three dimensional, two-temperature numerical study of a conceptual aeroshell by Fujita et al. in 2012 [1]. Use of the available afterbody heating flight data was carried out by Potter et al. in 2013 for the Viking entry vehicle [3]. Their results showed that the discrepancy in heat flux between the flight data and the postflight CFD analysis is caused by the disregard of the radiative heating. The most recent numerical work on simulating the afterbody radiation during Mars entry was done by Brandis et al. in 2015 [2]. The analysis was conducted for the Phoenix and MSL aeroshell at various trajectory points and the results showed that the tangent slab method cannot be used to calculate the afterbody radiation because it significantly overestimates the radiation. Hence, the full angular integration method must be used.

Experiment Methodology

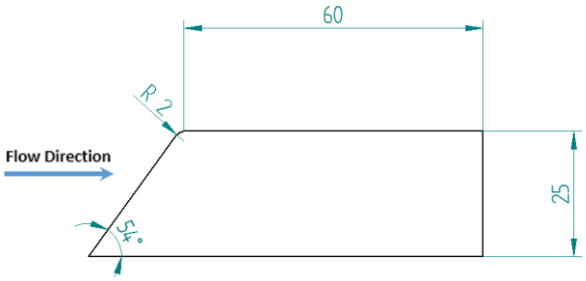

Figure 1. 2d test model geometry with a width of 100mm. Dimensions shown are in mm and degrees.

The X2 expansion tube [7] is selected as the preferred facility to perform the experiments. It is preferred over the reflected shock tube because it generates a freestream with less thermochemical excitation. For many representative trajectories, the afterbody radiation during Mars entry is strongest at around 3-4 km/s. Hence, three different velocity conditions, nominally at 2.8 km/s, 3.4 km/s, 4.0 km/s, are developed in the expansion tube to study the radiating expanding flow. The freestream pressure of the conditions were made such that a similarity in carbon dioxide number density is obtained with the expanding flow around the afterbody of an aeroshell in flight. The test model used is a two dimensional oblique shock expansion wedge model and it is shown in Figure 1. The desired expanding flow is created around the convex corner and it simulates the radiating expanding flow around the afterbody of an aeroshell during Mars entry.

Analyses of the Expansion Tube Test Conditions

Quality of the Generated Freestream Conditions

Three conditions were developed in the X2 expansion tube for the present study. In order to assess whether or not the freestream conditions are of sufficient quality for model validation it is necessary to evaluate the steady flow duration, shot-to-shot consistency and the size of the core flow.

Pitot probe measurements at different radial locations on the nozzle exit plane were used to investigate the steady flow duration and the core flow size. The results showed that the steady flow durations of all three conditions are sufficient for generating a steady flowfield around the test model; the 2.8 km/s condition had a steady time of 250 μs the 3.4 km/s condition had a steady time of 210 μs and the 4.0 km/s condition had a steady time of 140 μs. Additionally, the result showed a core flow size of at least 108 mm for all three conditions. Since the width of the two dimensional model used is 100 mm, the core flow size is large enough to accommodate the test model. CFD simulations of the test model will be carried out in the future to investigate the edge effects of the test model.

Measured shock speeds, acceleration tube wall pressure, nozzle exit pitot pressure and radiation measurements in the flowfield around the test model were used to assess the shot-to-shot consistency of the conditions. The subsequent results showed excellent repeatability of the conditions as the variations in the measured variables were under 10%.

Characterization of the Generated Freestream Conditions

It is necessary to accurately determine the state of the test flow exiting the nozzle for each experimental condition. An estimate of the freestream state can be made by using the PITOT code [8]. The PITOT code is a zero dimensional code which solves for the flow properties of the driver, test and accelerator gas at different states during the process of producing the hypervelocity test flow in the expansion tube. The PITOT code simulates the expansion tube processes by using isentropic expansion and compressible flow relations.

The unsteady expansion process is tuned to match the measured wall pressure in the acceleration tube. Also the steady expansion through the nozzle is tuned to match the average of the measured conical pitot probe pressure. This subsequently results in an estimate of the freestream condition. A comparison with the measured flathead pitot probe pressure will give an indication of the accuracy of the estimated freestream condition. The conditions in the current work yielded excellent agreement, within 10%, between the average of the flathead pitot probe measurement and the calculated pitot pressure using the estimated freestream condition. Hence, it is believed that the resulting freestream estimate is accurate. Furthermore, for the condition concerned in the current work, the two tuning variables were found to remain constant. This allows individual estimates of the freestream to be made for every run.

To rigorously assess the accuracy of the estimate from the PITOT code, various numerical studies are conducted. The uncertainty with the estimates of the PITOT code results from the expansion processes the test gas encounters as it travels through the acceleration tube and nozzle in which it may encounter non-equilibrium thermochemistry as well as viscous effects.

To investigate the effects of thermochemical non-equilibrium, freestream estimates were calculated with both the frozen and equilibrium limits in the PITOT code. This gives the bounding solutions for the freestream estimate due to the thermochemical influences. The shock wave measurements from the particular pitot survey shots x2s2906(2.8 km/s), x2s2905(3.4 km/s) and x2s2904(4.0 km/s) are used for this analysis. The frozen estimate of the freestream was calculated based on freezing the test gas at the stagnated state in the shock tube by assuming calorically perfect gas for the expansions, while the equilibrium limit was calculated based on equilibrium calculations of each state of the test gas as it travels through the expansion tube. The result of this analysis is summarized in Table 1. The results show that the frozen and equilibrium bounds of the tuned solutions are not significantly large for the estimated macroscopic flow properties of pressure, temperature, velocity and the frozen speed of sound. The bounds for the 3.4 km/s and 4.0 km/s conditions are particularly small while the 2.8 km/s condition showed a slightly larger bound. It can be inferred from the results that any thermochemical non-equilibrium involved would not have too great of an effect on the macroscopic flow properties. This is a positive result as it consequently allows the thermochemical state of the freestream to be estimated separately from the macroscopic state. As shown on Table 1, a large bound exists for the vibrational and chemical state of the freestream. Hence, it is important to determine the vibrational and chemical state and this is discussed further in the next section.

To investigate the effects of viscosity on the freestream estimates, an analysis is conducted by comparing the PITOT estimates to two-dimensional axisymmetric viscous CFD simulations of the acceleration tube and nozzle. The stagnated test gas condition in the shock tube is used as the inflow for CFD. CFD was conducted using the Eilmer3 code [9]. The particular pitot survey shots x2s2906(2.8 km/s), x2s2905(3.4 km/s) and x2s2904(4.0 km/s) are analyzed and the results are shown in Table 2. Excellent agreement is shown for the frozen speed of sound and velocity for all three conditions. Excellent agreement for the pressure is shown for the 2.8 km/s condition, while reasonable agreement is shown for the 3.4 km/s condition. Reasonable agreement is seen for the temperature estimate for all conditions, while the only poor agreement is for the estimate of the pressure for the 4.0 km/s

Condition	Code	P_{static} (Pa)	T (K)	a $(\frac{m}{s})$	V $(\frac{m}{s})$	T_v(K)	CO_2 Mole Fraction
Slow	Perfect Gas	355	1191	507	2877	2358	0.92
	Equilibrium	323	1010	474	2809	1010	1.0
	% Difference	9.9	17.9	6.9	2.4	133	-8
Medium	Perfect Gas	360	1378	560	3484	2758	0.76
	Equilibrium	341	1403	555	3490	1403	1.0
	% Difference	5.5	-1.7	0.9	-0.1	96	-24
Fast	Perfect Gas	150	1281	543	4077	2815	0.73
	Equilibrium	139	1301	536	4091	1301	1.0
	% Difference	7.9	-1.5	1.3	-0.3	116	-27

Table 1. Comparison between equilibrium and calorically perfect gas freestream estimates.

condition. This shows that the assumption of isentropic expansion in the PITOT code is a good assumption. Hence, tuning the isentropic expansions to the measured pressures adequately simulates the expansion processes in the facility.

Condition	Code	P_{static} (Pa)	T (K)	a $(\frac{m}{s})$	V $(\frac{m}{s})$
Slow	Eilmer	309	1154	505	2760
	PITOT	323	1010	474	2809
	% Difference	4.3	-14.2	-6.5	1.7
Medium	Eilmer	383	1606	588	3355
	PITOT	341	1403	555	3490
	% Difference	-12.3	-14.4	-5.9	3.8
Fast	Eilmer	97.4	1418	557	3893
	PITOT	139	1301	536	4091
	% Difference	30.1	-8.9	-3.9	4.8

Table 2. Comparison between PITOT and CFD freestream estimates.

It should be noted that the freestream estimate made by PITOT is believed to be the better representation of the actual freestream because it is tuned to match the measured PITOT pressures. Consequently, in the future, interpretations of radiation measurements will be carried out using the PITOT estimates.

Freestream Excitation

Review of previous work [10, 11, 12] had shown that similar freestream test conditions as the ones presented in this work, generated in other impulse facilities, suffer from freezing at an excited nonequilibrium thermochemical state. To investigate the thermochemical state of the freestream in the current work, a shock wave comparison is conducted for the freestream conditions in the present work. Numerically estimated shock waves using both the equilibrium and perfect gas estimate of the freestream conditions are compared with the measured shock wave of the wedge model. This is shown in Figure 2. The result revealed that the freestream condition concerned is frozen at an excited thermochemical state. The equilibrium freestream estimate significantly under-predicts the shock standoff, whereas the frozen freestream estimate gives a good match for the shock wave. This means that the thermochemical state of the test gas could be frozen at its state behind the reflected shock. In future work, emission spectroscopy will be performed on the freestream to confirm this finding.

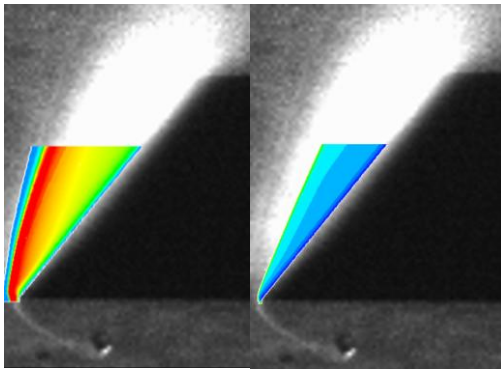

Figure 2. Shock Wave comparison of the 3.4 km/s velocity condition with (left) frozen freestream, and (right) equilibrium freestream.

Preliminary Infrared Radiation Measurements

As the flow was expected to produce radiation in the mid-infrared region, an infrared sensor was used to measure the radiation emission at various locations in the flowfield generated around the test model. The detector is an intrinsic InSb photoconductive detector and it is sensitive to radiation with wavelength between 1 µm and 5 µm. The measurements were made perpendicular to the flowfield and are focused using a lens, as shown on figure 3 (left). The square points on figure 3 (right) marks the measured locations in the flowfield. The locations were estimated to approximately represent three points on each of the two streamlines; a top and bottom streamline. On each streamline, a measurement was taken in the shock layer, the expansion fan centre and further down the back. Each pair of the top and bottom measurement is aligned in the same horizontal position as illustrated by the dashed line on figure 3 (right).

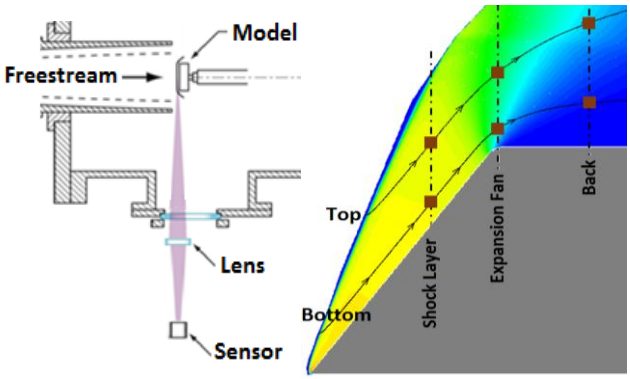

Figure 3. The infrared emission experiment (left) setup and (right) measurement locations.

Some interesting observations can be made by comparing the readings of the sensor at different locations in the flowfield and for different freestream conditions. The results showed that, at all the measured locations, the strongest radiation is produced by the 3.4 km/s freestream condition, while the weakest is produced by the 2.8 km/s freestream condition. Normalizing each streamline measurement with respect to its corresponding shock layer value, presented on figure 4, shows that the rate of decrease in radiation is greater on the bottom streamline. This is expected because the bottom streamline is subjected to more expansion due to the centred expansion fan from the convex corner. Furthermore, on the bottom streamline, the rate of decrease in radiation is the same for all three conditions. However, on the top streamline, the rate of decrease in radiation has more variation between the conditions. Additionally, on the bottom streamline, the intensity in the shock layer is about 5 times greater than the intensity at the back for all three conditions. Though, on the top streamline, the intensity of the shock layer ranges from about 2 to 1.2 times greater than the intensity at the back for the three conditions.

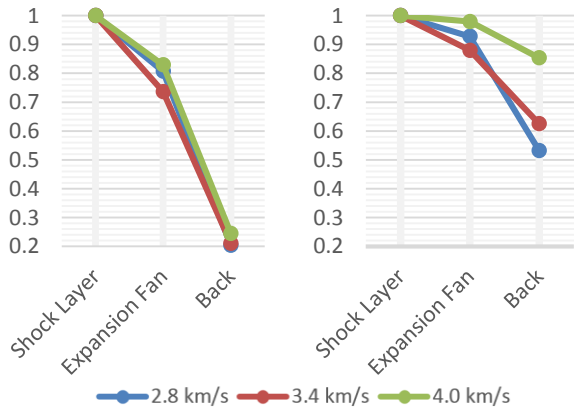

Figure 4. Radiation measurements normalized with respect to that of the shock layer for the bottom (left) and top (right) streamline.

In addition to assessing the magnitude of the point measurements, the data is also very useful in determining the steady duration of the flowfield because it shows the continuous measurement

throughout the duration of the test. A summary of the measured steady flow duration of the flowfield is presented in table 3. Determining the precise start and finish time of the steady duration is important for the purposes of conducting emission spectroscopy in the future. For all conditions, the measured steady duration of the flowfield is sufficient to obtain high quality emission spectroscopy data. While multiple repetitions of the same measurements showed excellent repeatability of the generated flowfield.

Condition	Streamline	Start	Finish	Duration
2.8 km/s	Bottom	266	380	114
	Top	238	356	118
3.4 km/s	Bottom	152	205	53
	Top	178	240	62
4.0 km/s	Bottom	83	165	82
	Top	102	180	78

Table 3. Summary of steady duration times. Time is given relative to shock arrival and has units of μs.

Future Work

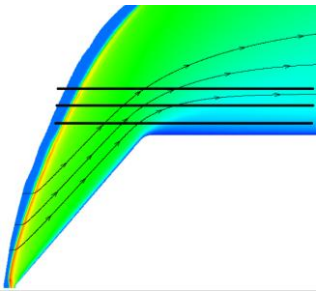

Figure 5. Locations of emission spectroscopy measurements.

Future work aims to provide benchmark experimental data to validate simulation tools and provide an appropriate uncertainty for flight missions. The survey of the previous research shows that there is no work done on comparing numerical models to ground test data in an expanding flow environment. In order to improve our current computational capabilities and reduce the uncertainties in the results, ground tests need to be conducted with the aim of acquiring high fidelity data.

In particular, emission spectroscopy will be conducted for the 2.7 μm and 4.3 μm bands of carbon dioxide which are the two most significant contributors of the afterbody radiation during Mars entry. Figure 5 shows the regions that are imaged in the emission spectroscopy measurements (represented by the horizontal black lines). The measurement covers the entire region from the shock wave to the back of the test model, through the expansion fan. Since the experimental set up only allows for one spatial direction, measurements from three locations at different heights above the test model in the expanding flow will be taken.

Conclusions

The motivation for studying the afterbody radiation during Mars entry has been discussed in this paper. The motivation has been supported by a brief literature review. An experiment has been designed to generate a flowfield with similarity of the carbon dioxide number density and vibrational temperature to the afterbody flowfield during Mars entry is created. The developed freestream conditions have been characterized. Additionally, preliminary radiation measurements of the generated expanding flow showed that the flow produces steady infrared radiation for a significant duration of time. This will allow for emission spectroscopy to be performed in the future.

References

[1] Fujita, K., Matsuyama, S., & Suzuki, T., "Prediction of Forebody and Aftbody Heat Transfer Rate for Mars Aerocapture Demonstrator," in *43rd AIAA Thermophysics Conference*, New Orleans, 2012.

[2] Brandis, A. M., Saunders, D., Johnston, C., Cruden, B., and White, T., "Radiative Heating on the After-Body of Martian Entry Vehicles," in *45th AIAA Thermophysics Conference*, Dallas, 2015.

[3] Potter, D., Karl, S., Lambert, M., & Hannemann, K., "Computation of radiative and convective contributions to Viking afterbody heating," in *44th AIAA Thermophysics Conference*, San Diego, 2013.

[4] Edquist, K. T., Dyakonov, A. A., Wright, M. J., and Tang, C. Y., "Aerothermodynamic environments definition for the Mars Science Laboratory entry capsule," in *45th AIAA Aerospace Sciences Meeting and Exhibit* , Reno, 2007.

[5] Lino Da Silva, M., & Beck, J., "Contribution of CO2 IR Radiation to Martian Entries Radiative Wall Fluxes," in *49th AIAA Aerospace Sciences Meeting including the New Horizons Forum and Aerospace Exposition*, Orlando, 2011.

[6] Gromov, V., and Surzhikov, S., "Convective and radiative heating of a martian space vehicle base surface," in *Fourth Symposium on Aerothermodynamics for Space Vehicles*, 2002.

[7] T. N. Eichmann, "Radiation measurements in a simulated Mars atmosphere," PhD Dissertation, Centre for Hypersonics, Department of Mechanical Engineering, University of Queensland, Brisbane, 2012.

[8] James, C., Gildfind, D., Morgan, R. G., Jacobs, P. A., & Zander, F., "Designing and simulating high enthalpy expansion tube conditions," in *APISAT 2013: 2013 Asia-Pacific International Symposium on Aerospace Technology*, 2013.

[9] Jacobs, P. A., Gollan, R. J., & Potter, D. F., "The Eilmer3 code: User guide and example book," The University of Queensland, St Lucia, 2014.

[10] Hollis, B. R., & Prabhu, D. K., "Assessment of laminar, convective aeroheating prediction uncertainties for Mars-entry vehicles," *Journal of Spacecraft and Rockets*, vol. 50, no. 1, pp. 56-68, 2013.

[11] MacLean, M., & Holden, M., "Numerical assessment of data in catalytic and transitional flows for Martian entry," in *9TH AIAA/ASME Joint Thermophysics and Heat Transfer Conference*, San Francisco, 2006.

[12] MacLean, M., Dufrene, A., & Holden, M., "Spherical Capsule Heating in High Enthalpy Carbon Dioxide in LENS-XX Expansion Tunnel," in *51st AIAA Aerospace Sciences Meeting and Exhibit, AIAA Paper*, 2013.